Understanding the ductility versus toughness and bendability decoupling of large elongated and fine grained Al 7475 - T6 alloy

Matthieu B. Lezaack[a], Florent Hannard[a], Aude Simar[a]

[a] Institute of Mechanics, Materials and Civil Engineering, Université catholique de Louvain, 1348 Louvain-la-Neuve, Belgium

Corresponding author: Matthieu B. Lezaack,
Place Sainte Barbe, 2 bte L5.02.02, 1348 Louvain-la-Neuve, Belgique
E-mail corresponding author: matthieu.lezaack@uclouvain.be

Abstract

7XXX aluminium alloys are widely used in aerospace components due to their high strength to weight ratio. However, first generation 7XXX alloys had a limited toughness and crack propagation resistance. New generation of 7XXX alloys succeed to increase material toughness, by playing on both alloying elements composition and purity level. One of the toughest alloy is the 7475 Al alloy, with a fracture toughness (K_{Ic}) that reaches up to 60 MPa√m in T6 conditions. Friction stir processing (FSP) is applied to 7475 Al rolled plates in order to generate a fine-grained microstructure. Heat treatments (HT) are performed in order to set rolled and FSPed microstructures into T6 peak-aged condition. While the T6 FSPed microstructure shows a significant fracture strain improvement in uniaxial tensile loading, this microstructure does not improve the crack propagation resistance compared to the T6 rolled material, neither on compact tension nor on bending specimens. Which mechanisms are responsible for this effect? A decoupling between ductility and toughness in 7XXX aluminium alloys is unexpected and the understanding of this phenomenon is of prime importance for mechanical design. This work reveals the competing effects of the FSPed microstructure on crack initiation and crack propagation. FSPed material delays the crack initiation under loading but the FSPed fine grains favour fully intergranular crack propagation. In comparison, the energy needed for the crack to cut through or circle around the rolled elongated grains is much higher in the rolled material. Indeed, elongated rolled grains act as crack arresters when the crack direction is perpendicular to the grain's main axis. In this case, failure of the rolled material leads to extensive transgranular propagation, increasing the energy absorption and rising the K_{Ic} values to higher levels. This work illustrates the formation and propagation of cracks in the rolled and FSPed 7XXX alloys microstructures in order to explain the damage sequence and the competition between transgranular and intergranular failure.

Key words

Toughness, Ductility, Bending, Friction Stir Processing (FSP), Damage mechanisms, Formability, Aluminium alloys 7XXX.

Highlights

- FSPed T6 7475 Al alloy has high ductility but low K_{Ic} compared to rolled T6 plate.
- Ductility vs toughness decoupling is related to the sequence in damage mechanism.
- FSPed T6 7475 alloy delays damage initiation.
- Intergranular crack propagates easily in FSPed T6 alloy after crack initiation.
- Rolled T6 7475 alloy deviates cracks easily, leading to higher toughness.

1. Introduction

7XXX aluminium alloys are reaching high strength thanks to the addition of zinc, magnesium and copper to the aluminium matrix. 7XXX Al alloys are heat treatable. In the hardest conditions, called T6 state, a fine hardening precipitation composed of $MgZn_2$ precipitates is formed. The precipitates observed are a mixture of η' and η precipitates, as described by Su *et al*.[1] and Wang *et al.* [2]. Liu *et al.* have demonstrated the sensitivity of the homogeneity of the hardening precipitation of 7XXX Al alloys to heat cycles [3]. In peak aged T6 state, precipitate free zones (PFZ) are observed at grain boundary vicinity due to the formation of coarser precipitates on the grain boundaries by preferential precipitation, as described by Rometsch *et al*. [4]. The width of PFZ and size of coarse precipitates is quench sensitive [3][4]. Effects of quench on 7XXX alloys precipitates and mechanical properties were recently reviewed by Milkereit *et al.* [5]. Due to this T6 microstructure, strength is increased at the expense of ductility and toughness, in particular for the first generation of 7XXX alloys [6][7]. Crack propagation resistance is a key parameter in structural design as some defects and cracks are usually generated during manufacturing [8]. In particular, some impurities are remaining from alloy casting, generating brittle intermetallic (IM) particles [9]. These particles are either iron-rich or silicon-rich phases and play a crucial role on damage mechanisms by nucleating cavities and cracks by their fracture or decohesion with the matrix [6]. Iron-rich intermetallic particles have been described as Al_7Cu_2Fe phase by Li *et al.* [10]. More recent 7XXX aluminium alloys, such as the 7475 alloy, now widely used in the aerospace industry, were thus developed for improving both crack initiation and crack propagation, as well as for resisting corrosion and lowering heat sensitivity [7].

1.1. Mechanism of crack propagation

A crack generates local stress concentration that decreases away from the crack tip vicinity [8]. The crack tip opening distance (CTOD), i.e. the sharpness of the crack, affects the local stress state [8]. A sharper crack rises stress concentration [11]. The stress intensity factor K (MPa√m) characterizes the stress state in front of crack tip. In plane strain, the critical K value (K_{Ic}) is used to evaluate the toughness of the material. K_{Ic} corresponds to the stress state that minimizes the crack propagation resistance, in presence of a sharp crack, see ASTM E399 standard procedure. To ensure valid measurements and sufficient crack length, K_{Ic} evaluation procedure requires fatigue pre-cracked samples according to ASTM E399.

The sharpness of the crack or crack tip opening is an important parameter. Vratnica *et al.* [11] have proposed a study on bending notched samples made of overaged 7XXX Al alloy. The notch stress intensity factor K is proportional to the square root of the notch radius and the plastic zone size is increasing with increasing notch radius [11]. The resistance to crack propagation is thus increasing with larger notch radius, because a larger plastic zone will form in front of the crack tip [11].

1.2. Microstructural features influencing the competition between the inter / transgranular crack propagation in 7XXX alloys

Table 1 summarizes the mechanical properties and damage mechanisms reported in literature for 7XXX aluminium alloys. Vratnica *et al.* [11] noticed that impurities like iron-rich IM particles and coarse secondary phases influence the crack propagation mechanisms depending on the size of the plastic zone in front of the notch. Small plastic zone associated to sharp notch leads to more transgranular propagation [11]. Indeed, as the IM particles interspacing is much larger than the size of the plastic zone, no breakage of IM particles is observed leading to a flat and smooth crack surface [11]. Oppositely, a larger plastic zone in front of a smoother notch is associated to IM particles fracture and facilitates intergranular crack propagation [11]. In this second case, the crack propagation mode is both intergranular and transgranular leading to a rougher cracked surface, as noticed in Table 1. The influence of intermetallic particles was also demonstrated by Kamp *et al.* on 7449 and 7150 Al alloys [12]. Intermetallic particles lead to significant and coarse ductile damage nucleation, becoming predominant for overaged T7 conditions [12]. According to Kamp, this coarse void nucleation mechanism influences the crack path, as well as the competition between intergranular and transgranular crack propagation modes.[12].

<table>
<tr><th>Reference</th><th>Alloy [wt%]</th><th>State</th><th>σ_y [MPa]</th><th>K_{Ic} [MPa√m]</th><th>Dominant damage mechanism</th></tr>
<tr><td rowspan="3">Ludkta et al. [6]</td><td>7075 (2.2 Mg + 5.6 Zn)</td><td>T6</td><td>496</td><td>102</td><td>Transgranular</td></tr>
<tr><td>(2.8 Mg + 7.0 Zn)</td><td>T6</td><td>583</td><td>52</td><td>Intergranular</td></tr>
<tr><td>(2.8 Mg + 7.8 Zn)</td><td>T6</td><td>602</td><td>39</td><td>Intergranular</td></tr>
<tr><td rowspan="3">Vratnica et al. [11]</td><td rowspan="3">(2.3 Mg + 7.3 Zn)</td><td>T73</td><td>283</td><td>46</td><td></td></tr>
<tr><td>T73 + sharp notch</td><td></td><td></td><td>Transgranular</td></tr>
<tr><td>T73 + smooth notch</td><td></td><td></td><td>Intergranular & Transgranular</td></tr>
<tr><td rowspan="9">Kamp et al. [12]</td><td rowspan="2">7150 (2.3 Mg + 8 Zn)</td><td>T6</td><td>600</td><td>31</td><td rowspan="9">Intergranular & Transgranular</td></tr>
<tr><td>T7</td><td>570</td><td>30</td></tr>
<tr><td rowspan="7">7449 (2.3 Mg + 6.2 Zn)</td><td>T6</td><td>630</td><td>25</td></tr>
<tr><td rowspan="6">T7 (Decreasing over aging)</td><td>400</td><td>45</td></tr>
<tr><td>420</td><td>44</td></tr>
<tr><td>425</td><td>43</td></tr>
<tr><td>470</td><td>39</td></tr>
<tr><td>512</td><td>34</td></tr>
<tr><td>585</td><td>31</td></tr>
<tr><td></td><td></td><td></td><td>590</td><td>28</td><td></td></tr>
<tr><td rowspan="2">Tajally et al. [14]</td><td>7075 (2.5 Mg + 5.6 Zn)</td><td>O</td><td>125</td><td rowspan="2"></td><td rowspan="2">Transgranular</td></tr>
<tr><td></td><td>O + cold rolling</td><td>275 to 310</td></tr>
<tr><td rowspan="2">Iriç et al. [15]</td><td rowspan="2">7075 (2.8 Mg + 5.9 Zn)</td><td>T6 (T - dir)</td><td rowspan="2"></td><td>29</td><td rowspan="2"></td></tr>
<tr><td>T6 (L - dir)</td><td>22</td></tr>
<tr><td rowspan="2">Wang et al. [16]</td><td>(1.8 Mg + 6.1 Zn)</td><td>RRA</td><td>552</td><td rowspan="2"></td><td>Intergranular</td></tr>
<tr><td>(1.8 Mg + 6.1 Zn + 0.10 Er)</td><td>RRA</td><td>622</td><td>Transgranular</td></tr>
</table>

Table 1: Literature review on the mechanical properties of 7XXX alloys and damage mechanisms. Zn and Mg alloying elements in weight %. O, T6, T7 and Retrogression and Re-Aging (RRA) tempers were studied. Yield stress (σ_y) and toughness (K_{Ic}) are displayed if provided. The dominant damage mechanism (right column) refers to the surface aspect of broken samples: if grain decohesion is massively observed, then, the intergranular mechanism dominates, while grain interior failure of the material is associated to transgranular mechanism.

Flow properties of the matrix also affect the crack propagation. Ludkta *et al*. [6] have demonstrated the influence of alloying element content on crack propagation mechanisms. Higher solute content in 7XXX Al series (i.e. higher amount of Mg and Zn, see Table 1) leads to higher strength in T6 condition, associated to lower fracture toughness and lower tearing resistance [6]. Highly alloyed materials show quasi-brittle intergranular failure and lower toughness in peak aged conditions [6]. However, Ludkta *et al.* [6] have shown that alloys with intermediate and low alloying elements content have the same proportion of transgranular and intergranular crack propagation ratio despite different toughness. Ludtka *et al.* [6] proposed that micro slip bands of the matrix under straining and large yield stress difference between PFZ and matrix are both drastically decreasing the toughness by favouring fracture initiation. Higher alloying element content materials have coarser matrix slip bands, generating larger strain localization at grain boundaries, while the lower alloying element content alloys presents grain boundaries that accommodates better to matrix slip bands [6]. Mechanically speaking, intergranular damage is favoured when the difference between matrix and PFZ yield stresses is increasing [6]. This was also modelled by Scheyvaerts *et al.* [13], who demonstrated that intergranular damage occurs preferentially with increasing matrix to PFZ yield stress ratio.

Beside chemical composition, crack propagation in 7XXX Al alloys is sensitive to heat treatment [4][5]. Tajally *et al*. [14] studied 7075 alloy under solid solution of the alloying elements after annealing (i.e. under an O state), see Table 1. Tajally *et al.* [14] investigated the influence of cold rolling of 7075 O alloy on impact energy. In O state, the influence of the PFZ and hardening precipitates on the damage mechanisms is inhibited as the solute elements are homogeneously dissolved in the Al matrix [14]. Annealing the 7075 alloy is associated to an increase in ductility and impact energy, as the grain boundary preferential failure is inhibited in O state [14]. However, cold rolling after annealing is reducing impact energy as well as the ductility due to excessive strain hardening [14]. The cold-rolled microstructure presents a quasi-brittle transgranular fracture propagation (despite a yield stress 300 MPa lower than in [6]). Within 7449 and 7150 Al alloys, Kamp *et al.* [12] observed that K_{Ic} is linearly decreasing with yield stress for yield stress ranging from 400 to 625 MPa, see Table 1. The overaged T7 state is thus presenting lower yield stress but higher toughness than the peak-aged T6 state [12].

Crack propagation resistance is also dependent on the grain structure in 7XXX Al alloys. Iriç *et al.* [15] have observed that toughness is highly sensitive to Al plate anisotropy. Indeed, elongated rolled grains are efficient to retard crack propagation when the crack is propagating perpendicular to the grain main axis [15]. Transgranular propagation is thus favoured across these elongated grains, increasing the amount of energy dissipated during the damage process, in accordance with the results of Ludkta and Laughlin [6]. Oppositely, cracks parallel to the elongated grains are propagating more easily in an intergranular mode, associated with limited energy absorption [15]. According to Iriç *et al.* [15], a 25% decrease of K_{Ic} was observed on an industrial 7075 alloy, when comparing the crack propagation along the rolling direction (21 MPa√m) to propagation in the transverse direction (29 MPa√m), see Table 1. Anisotropy of the 7XXX alloys is also evidenced in uniaxial tensile loading [15]. Similarly, Tajally *et al.* [14] showed that maximum strength was obtained when loading along the transverse direction after cold rolling.

Besides the influence of grains anisotropy on toughness, the mechanisms of crack propagation are also sensitive to grain size and to the degree of recrystallization [16]. Wang *et al.* [16] have studied the sensitivity of damage mechanisms to the microstructure of partially recrystallized 7XXX Al alloys. The un-recrystallized elongated grains (obtained by adding Er-rich dispersoids) are associated with transgranular crack propagation, while smaller equiaxed recrystallized gains are leading to intergranular crack propagation under tensile loading, see Table 1 [16].

1.3. How can toughness be increased in 7XXX aluminium alloys?

In the second generation of 7XXX alloys (e.g. 7475, 7055, 7085), high toughness and high strength combinations were obtained by modifying the alloy chemical composition [7]. For instance, the 7475 alloy can reach a K_{Ic} above 50 MPa√m [7]. Higher toughness alloys were also developed by avoiding microstructural heterogeneities [12]. In a 7449-A alloy, a lower volume fraction of coarse IM particles and coarse secondary phases is leading to significantly higher K_{Ic} values compared to IM richer 7449 reference alloy, as observed by Kamp *et al.* [12].

Nevertheless, these high toughness 7XXX Al alloys still keep their low ductility, limiting their crashworthiness, as well as their formability. The damage sequence is rather complex in the 7XXX Al alloys [6]. It is generally observed that damage initiates on IM particles, either by particles fracture or decohesion from the matrix [6][12]. In our previous study, the combination of Friction Stir Processing (see the review by Mishra *et al.* [17] for further information on FSP) and Heat Treatments (HT) was studied. FSP was already investigated on 7XXX alloys, revealing systematic softening of processed material due to coarsening of the hardening precipitates [1][18]. Post-processing HT were then applied in order to regenerate the hardening precipitates. Combining FSP and HT on 7475 alloy was shown to lead to a significant 180% ductility improvement in terms of fracture strain while maintaining the T6 yield stress unchanged compared to the initial rolled microstructure [19]. Due to similar HT applied on initial and processed 7475 alloys, hardening precipitates and PFZ width are similar in both FSPed and rolled microstructures [19]. The resulting precipitation corresponds thus to the T6 peak strength condition [19]. Same trends were obtained on the FSPed 7075 Al alloy, but with a 150% ductility improvement in T6 state [19]. The mechanisms leading to this improvement were identified as the delay of void initiation on coarse IM particles and the subsequent limitation of damage coalescence within clusters of IM particles [19]. Indeed, FSP refines the microstructure as only 1% of the IM particles are greater than 5 µm after 2 passes FSP Compared to 15% in the initial rolled alloy [19]. The reduction of IM particle size increases the plastic deformation before void nucleation and microcracks propagation, as observed and described by Hannard *et al*. [20].

The goal of this study is to investigate the effect of microstructural refinement due to FSP under various loading conditions. Toughness and formability will be studied by the testing of bending and compact tension (CT) specimens, respectively. Our previous work detailed the damage sequence under uniaxial tensile loading in link with the microstructural features [19]. After void nucleation, damage grows until coalescence of porosities, typically starting first at preferential locations such as clusters of iron rich particles [6][19][20]. Mixed inter / transgranular nature of the crack propagation was observed on broken surfaces, as already observed in 7XXX alloys by several authors [6][12][19]. The purpose of the present work is thus to study the crack propagation mechanisms under different loading conditions and to distinguish the impact of grain refinement on crack formation and propagation.

2. Materials and methods

Industrial rolled plates of 7475 Al alloy in T7351 overaged state were selected in 12 mm thickness. The subsequent samples denomination refers to the initial rolled material crystallographic orientations: S-L-T for the short, rolling and transverse directions respectively. Inductively coupled plasma (ICP) spectroscopy is used for chemical composition identification and the results are provided in Table 2.

Chemical composition %wt											
	Al	Zn	Mg	Cu	Fe	Cr	Mn	Si	Ti	Ga	Zr
Al 7475	90.0	5.67	2.20	1.51	0.08	0.22	0.01	0.04	0.04	0.01	0.01

Table 2: Chemical composition of studied 7475 Al alloy.

Friction stir processing (FSP) is applied to 400 mm × 70 mm coupons. A H30 steel tri-flatted threated tool is used for processing the plate. The tool was composed of a shoulder of 22 mm diameter prolonged by a pin with 10 mm height, with root and reduced diameters of 10 mm and 6 mm, respectively. A dedicated FSW-P machine (TRA-C industries) is used under 300 RPM rotating speed and 100 mm/min advancing speed. Vertical force control is applied during processing, set to 15.5 kN. The FSP direction is parallel to the initial transverse (T) direction of the base rolled material (see Figure 1b).

Heat treatments (HT) are applied to both FSPed and rolled alloys, following an optimization detailed in [21]. A first solution heat treatment is performed at 470°C for 30 minutes, followed by water quenching. Then, aging treatment is performed at 120°C for 24h in order to reach the peak-aged T6 state. This two-step HT is denominated T6 HT.

Bending coupons of 2.5 mm × 15 mm × 70 mm are extracted out of the rolled and FSPed alloys, as displayed on Figure 1. The bending line is either parallel (RM L-S) or perpendicular to the rolling direction (RM T-S). The bending line is parallel to the FSP direction (FSP-S) for FSPed alloy, enforcing the bending inside the NZ. Three bending coupons are extracted in the plate thickness. According to grain size analysis performed in [21], the grain size is homogeneous through the entire NZ. A Zwick 50 kN machine associated to an adequate bending setup was used to bend the coupons until reaching 20% force drop. This setup is composed of two rollers and a knife. The distance between rollers centres is adjusted to the coupons thickness, following specifications of VDA 238-100 standard for metallic materials. Three samples are tested for each condition.

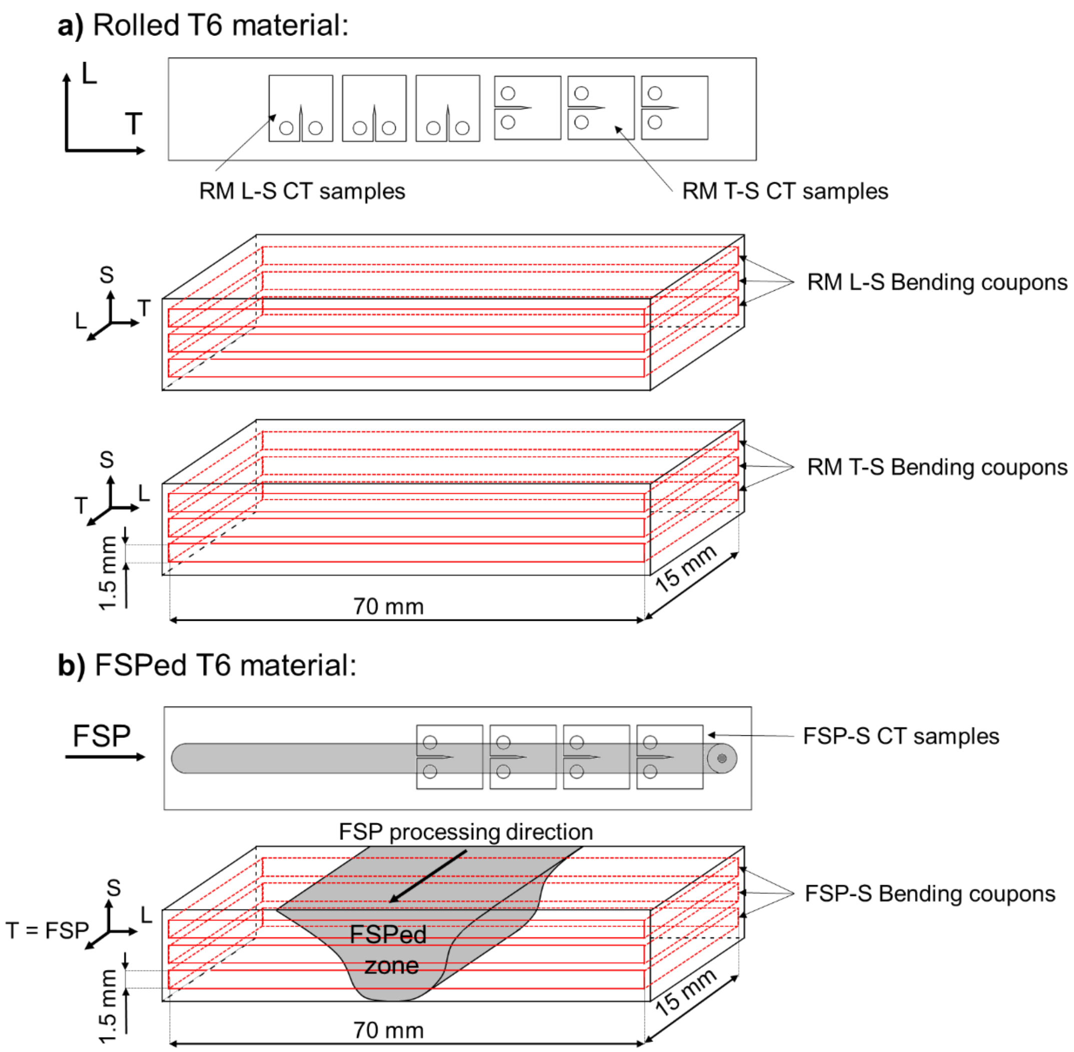

Figure 1: Bending coupons and CT samples definition in relation to the rolling or FSP directions. ***a)*** *CT samples are oriented with the pre-crack parallel to the rolling direction (L) or to the transverse direction (T). Concerning the bending coupons, three samples are extracted on the top of each other in the thickness direction (S). Again, the coupons orientation is following either the rolling direction (L) or the transverse direction (T),* ***b)*** *CT samples of FSPed material are extracted with pre-crack parallel to the processing direction. CT samples are extracted with the bending line located inside the nugget zone of the processed area.*

Compact tension (CT) samples are also extracted from both rolled and FSPed alloys, with the notch direction following the rolling direction (RM L-S), the transverse direction (RM T-S) and the FSP direction (FSP-S), see Figure 1. The detailed geometry of CT specimens is provided in supplementary Figure S1. The notches of the CT specimens were machined by electrical discharge machining and fatigue pre-crack is introduced in each sample prior to the loading procedure, using a 400 N - 4000 N alternating loading for 4000 cycles. A Zwick 250 kN machine was used for loading the CT samples, following E399 ASTM standards. In addition, elastic unloading steps were performed by steps of 50 µm of crack tip opening displacement (CTOD). The measured compliance of the samples allows computing the crack length at each unloading step following the E1820 ASTM standard. Three samples per condition are tested.

Material characterization was performed using optical microscopy (OM) and scanning electron microscopy (SEM) after standard polishing procedures. Keller's reagent is used for etching OM samples [18]. Broken samples are characterized using SEM fractography. Bending and CT samples are then cut at mid-thickness in order to observe the crack path and the grain morphology.

Image analysis of broken CT specimens was performed using ImageJ software. A "directionality analysis" was performed using the "Directionality plugin" of ImageJ [22]. This plugin allows the identification of preferential orientations within structures. In this work, the directionality of the samples broken surface is measured. See supplementary data Figure S2 for further explanations and examples. A representative 380 µm × 560 µm fracture surface was analysed in all conditions.

3. Results

3.1. FSP microstructure

The rolled 7475 Al alloy was successfully processed by FSP, i.e. without any processing defects like cavities, wormhole or cracks due to lack of plasticity or excessive or too low heating during the process [18], see Figure 2. Figure 2a shows the full processed plate cross-section, with the FSPed area at the centre, surrounded by unaffected material. Figure 2b highlights the typical processed zone structure, composed of the nugget zone (NZ) (also called stir zone (SZ)), the thermomechanically affected zone (TMAZ) and the heat affected zone (HAZ). Figure 2c illustrates the grain structure of the NZ presenting fine equiaxed grains, around 3 µm in diameter (see [21] for more details). Oppositely, rolled grains are hundreds of µm long in the rolling direction (L), 100 µm to 500 µm wide in transverse direction (T) and 25 to 50 µm thick in short direction (S), see Figure 3a,b.

FSPed grains (Figure 2c) are presenting coarse precipitates at grain boundaries associated with a softening of the NZ material, as shown in our previous study [21] and in the literature [1]. The 2-steps T6 HT allows to dissolve these precipitates and then to regenerate a finer precipitation [21]. The T6 HT is also applied to the initial rolled material. Both rolled and FSPed microstructures are thus similar in terms of T6 hardening precipitates and PFZ [19]. These T6 microstructures are thus available for bending and CT specimens. The yield stresses extracted from uniaxial tensile tests are given in Table 3, see [19] for more details. The material loaded along the rolling direction (RM - L) is showing a slightly lower yield stress (20 MPa lower) than when loading along the transverse direction (RM - T). FSPed material shows a strength similar to the transverse direction sample but a significant increase in fracture strain, up to 70% $\varepsilon_{fracture\ strain}$ after 2 pass of FSP (i.e. an increase of 180% compared to the rolled material loaded along the transverse direction, as recalled in section 1.3). The fracture strain is defined as $\varepsilon_{fracture\ strain} = \ln(A_0/A_f)$, with A_0 and A_f being initial and final sample cross section, see [19].

	RM - L direction	RM - T direction	FSP - Nugget zone	FSP (2 pass) - Nugget zone
σ_{yield} [MPa]	484.0 ± 2.9	503.7 ± 4.3	502.6 ± 4.6	507.8 ± 4.8
$\sigma_{ultimate}$ [MPa]	556.3 ± 1.1	588.3 ± 2.6	560.7 ± 3.8	565.0 ± 2.7
$\varepsilon_{necking}$ [-]	0.139 ± 0.002	0.126 ± 0.002	0.127 ± 0.004	0.124 ± 0.007
$\varepsilon_{fracture\ strain}$ [-]	0.396 ± 0.022	0.255 ± 0.017	0.540 ± 0.037	0.695 ± 0.029

Table 3: Tensile properties of studied materials in T6 state [19]. Yield stress: σ_{yield}, ultimate tensile stress: $\sigma_{ultimate}$, uniform elongation: $\varepsilon_{necking}$, fracture strain: $\varepsilon_{fracture\ strain}$.

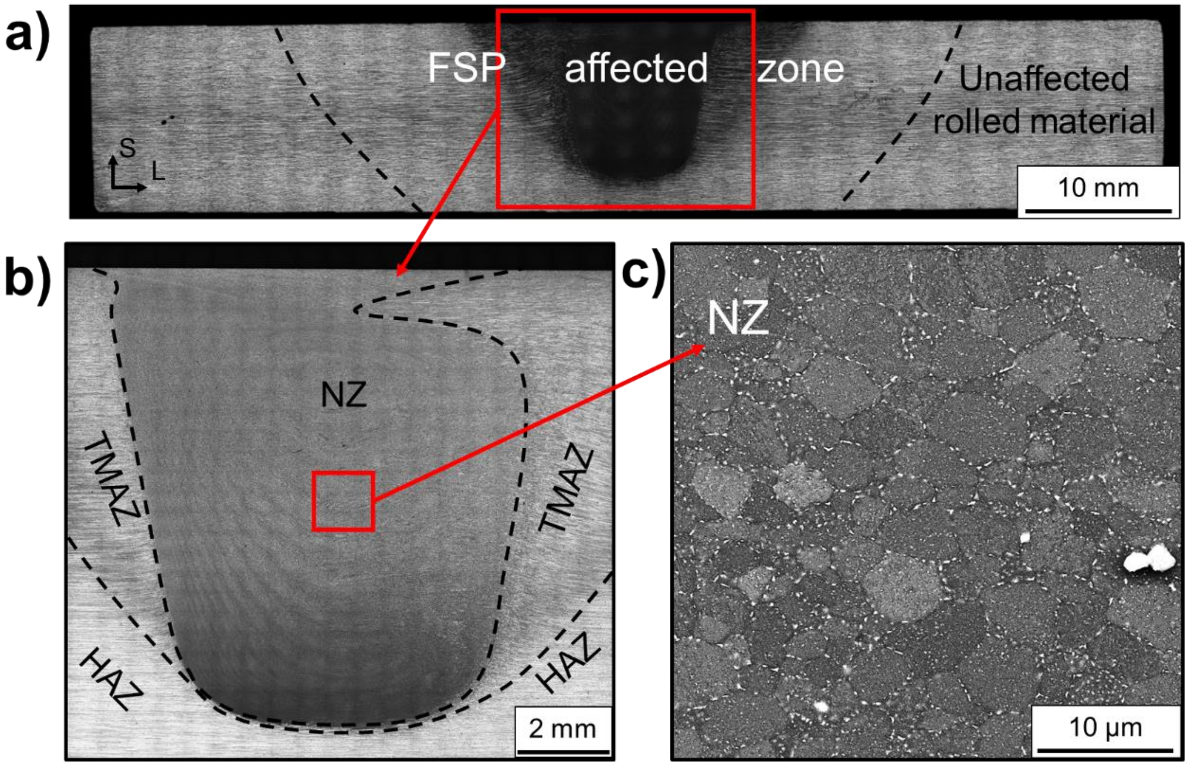

*Figure 2: Microstructure of FSPed processed zone in the base 7475 alloy. **a)** overview of FSPed zone inside rolled material coupon, **b)** higher magnification on the processed area, showing nugget zone (NZ) (also called Stir Zone (SZ)), thermomechanically affected zone (TMAZ) and heat affected zones (HAZ), **c)** FSPed alloy grains of NZ at high magnification.*

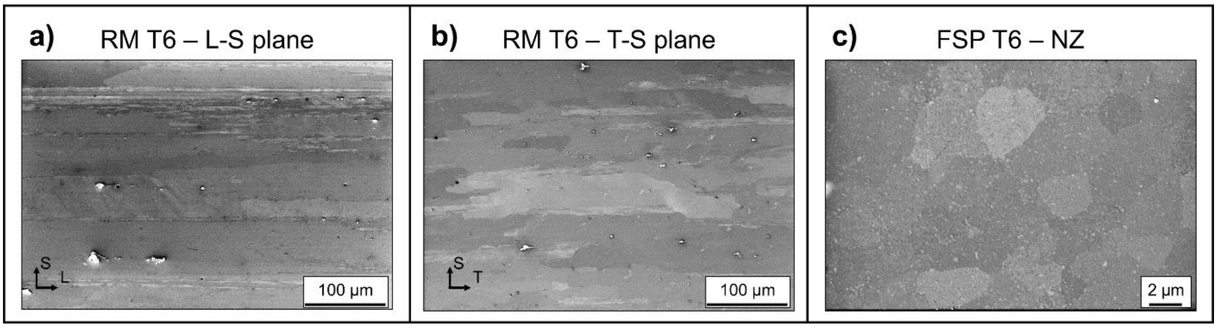

*Figure 3: 7475 alloy in T6 state after solution and aging heat treatments. **a)** RM in short-rolling (L-S) plane, **b)** RM in short-transverse (T-S) plane, **c)** FSP nugget zone (NZ) in T6 state, higher magnification on FSPed alloy due to grain refinement.*

Figure 3 displays the studied microstructures after the T6 heat treatment. Rolled material is characterized by elongated grains in the rolling direction as well as in the transverse direction. IM particles clusters are parallel to the rolling direction, see Figure 3a. Figure 3c shows the FSPed nugget zone after the T6 treatment. Coarse crown precipitates formed during FSP (see Figure 2c) have dissolved during the solution heat treatment at 470°C. Grains are not significantly changed after the T6 treatment, with a typical grain size of 3 µm. Note the higher magnification selected for the FSPed material image due to grain refinement.

3.2. Bending tests

Bending tests were performed on the three T6 materials characterized on Figure 3. Representative loading curves are shown in Figure 4a. The first alloy to fail (i.e. when the force decreases to as low as 80% of the maximal bending force) is the rolled material with the bending line parallel to the rolling direction (RM L-S). The samples with their bending line parallel to FSPed direction (FSP-S) and parallel to the transverse direction (RM T-S) display similar behaviour. This is confirmed on Figure 4b: the angle for which the maximal bending force is reached is greater in the T-S and FSPed samples. The RM L-S samples have lower bending angle at maximum strength.

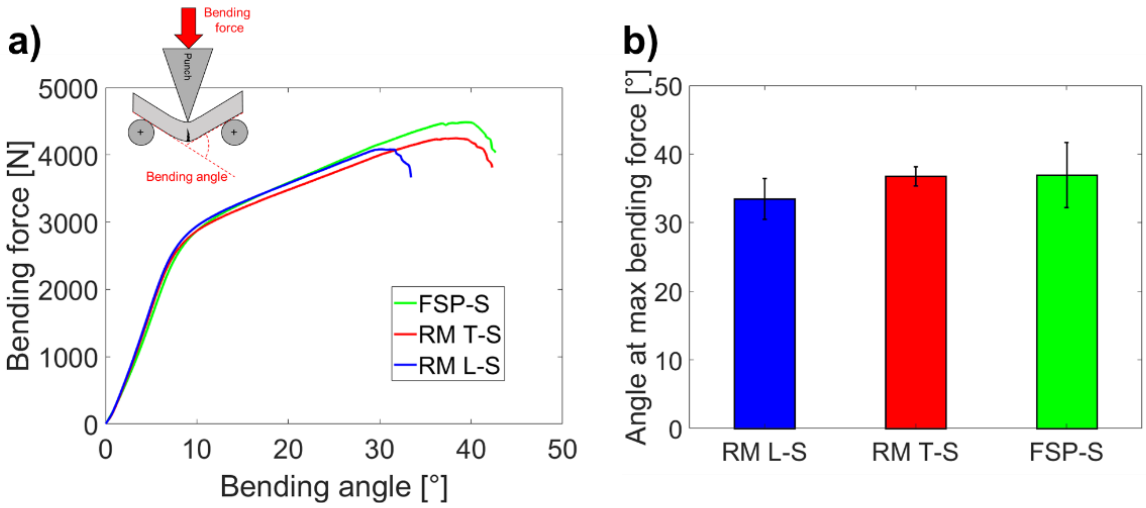

*Figure 4: **a)** Bending force versus angle diagram, bending setup is schematized on top left, rolled material with bending line parallel to the rolling direction (RM L-S sample) fails at lower angle values, **b)** bending angles at maximum force, the RM L-S samples reach lower angle while FSP-S and RM T-S specimens have similar angle at maximum bending force. FSPed and rolled materials are in T6 state.*

Figure 5 displays the cracked samples at low magnification after cutting and polishing the bending coupons. In Figure 5a, the rolled microstructure bended along the rolling direction (RM L-S) is showing a tortuous crack, nucleated on the right surface and growing in the thickness (S) direction. Similar observation are made in Figure 5b where bending is parallel to the transverse direction (RM T-S). Figure 5c displays the cracked FSPed material (FSP-S). The FSPed alloy crack is clearly longer than what is observed for the rolled samples, with limited macroscopic crack deviation.

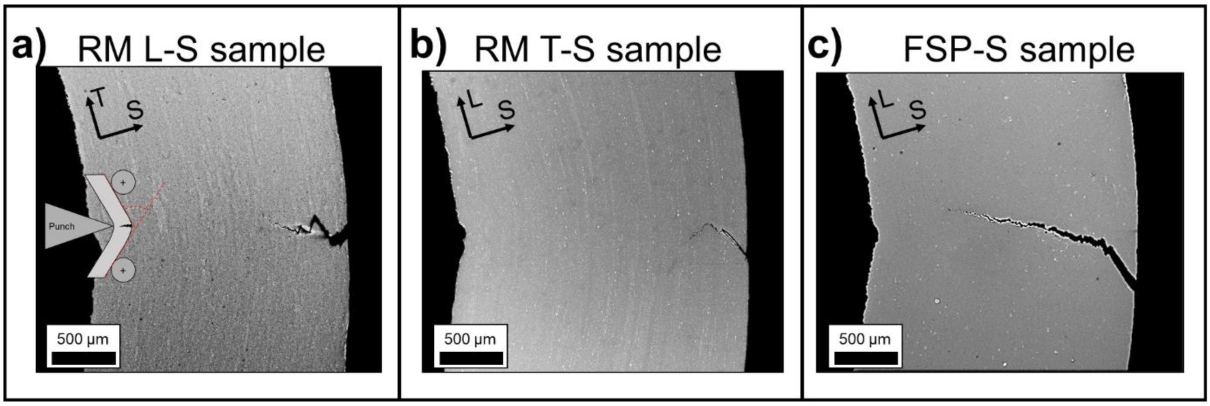

Figure 5: Bending coupons polished at mid-width after reaching 80% of the maximum bending force. ***a)*** *rolled material RM L-S sample, bending line parallel to rolling direction (L) and crack propagating in short direction (S),* ***b)*** *rolled material RM T-S sample, bending line parallel to transverse direction (T) and crack propagating in short direction (S),* ***c)*** *FSPed material FSP-S sample, bending line parallel to FSP processing direction and crack propagating in short direction (S).*

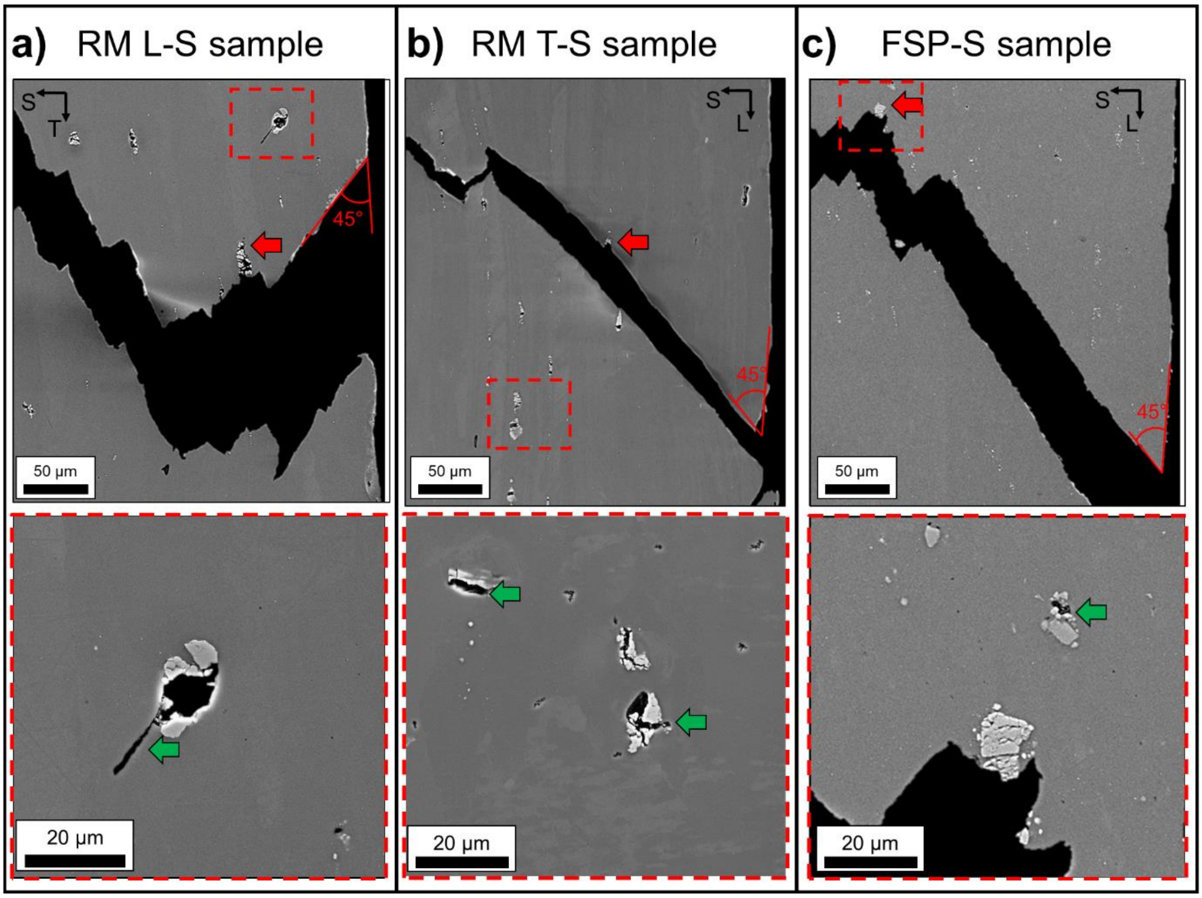

Figure 6: Bending coupons polished at mid-width after reaching 80% of the maximum bending force. Crack initiation region for all samples: ***a)*** *rolled material RM L-S sample,* ***b)*** *rolled material RM T-S sample,* ***c)*** *FSP-S sample. All samples present a 45° crack initiation direction with respect to sample surface. Red dashed boxes regions on top pictures are displayed at higher magnification on bottom. Red arrows indicate broken IM particles that are located on the crack path. Green arrows indicate damage and cracks at the vicinity of the main crack. The crack propagates from the right to the left of the figures. All samples are in T6 state.*

Figure 6a-b highlight the crack initiation region, i.e. near the tensile surface of the bending coupons, of the rolled alloys in RM L-S and RM T-S bending samples, respectively. A 45°

angle is associated with the crack initial propagation from the surface towards the inner plate. A similar 45° angle is measured for the FSPed microstructure, see Figure 6c. IM particles are distributed along the main crack path. Broken IM are also found in the vicinity of the main crack (see bottom figures). In Figure 6a (bottom), a microcrack has nucleated from a broken IM, following the 45° direction similarly to the main crack.

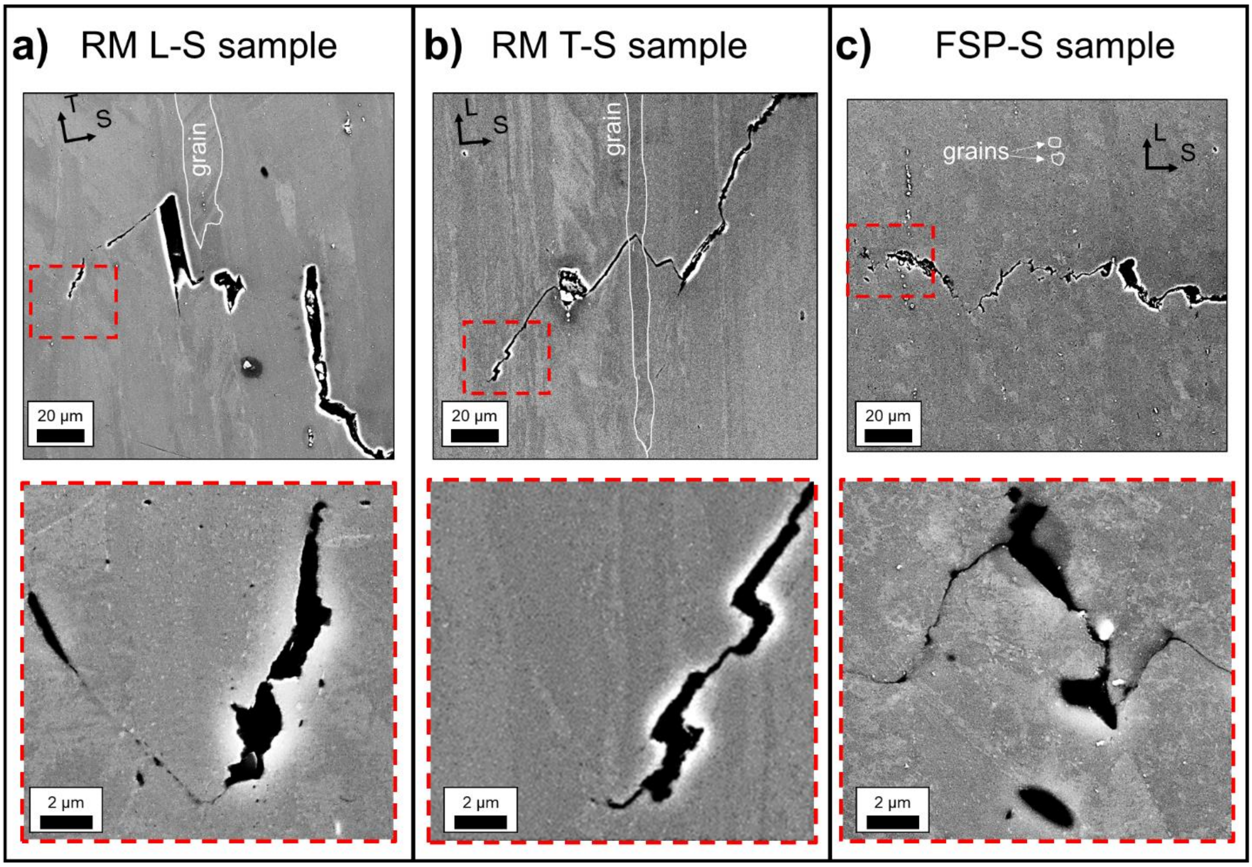

Figure 7: Bending coupons polished at mid-width after reaching 80% of the maximum force, highlighting the crack tip region. ***a)*** *rolled material RM L-S sample, bending line parallel to rolling direction (L) and crack propagating in short direction (S),* ***b)*** *rolled material RM T-S sample, bending line parallel to transverse direction (T) and crack propagating in short direction (S),* ***c)*** *FSP-S sample, bending line parallel to FSP processing direction and crack propagating in short direction (S). Red dashed boxes regions on top sub-figures are displayed at higher magnification on bottom sub-figures. The crack propagates from the right to the left of the sub-figures. All samples are in T6 state.*

Figure 7 presents the vicinity of crack tip at a higher magnification. On the three samples, the influence of grains and iron rich IM particles on the crack path is clear. IM are broken, even at some distance from the crack line. These broken IM influence the strain field in the surrounding matrix and interact with the plastic zone in front of the crack tip, which causes crack path deviation. This is in accordance with observations by Vratnica *et al.* [11].

Figure 7a shows some segments of the main crack, as well as some secondary cracks growing in a direction (T) perpendicular to the propagation direction (S). Crack deviation along the T direction follows the elongated grain boundaries. The main crack is thus composed of segments oriented into the T direction connected by straight sections tilted by approximatively 45° from the main propagation (S) direction.

On Figure 7b, bending the alloy along the transverse direction (RM T-S), i.e. tensile stresses along the rolling direction, leads to similar influence of the grain boundaries. Indeed, crack deviation is observed, either due to broken IM particles or grain boundary preferential failure - leading to vertical crack propagation. In this sample, grain boundary deviation is not as pronounced as in Figure 7a. Most of the crack path is composed of sheared grains at 45° from the loading direction, i.e. transgranular crack propagation.

In Figure 7c, the FSPed microstructure (FSP-S) does not show the same crack features. The crack has propagated without significant deviation when observed at lower magnification. The crack propagation in the refined FSPed microstructure is better observed at high magnification: the crack is contouring the grains while the remaining IM particles that were refined after FSP did not lead to significant crack deviation.

3.3. CT tests

Figure 8 shows the CT tests results. Figure 8a shows the testing setup and Figure 8b shows representative loading curves with elastic unloading steps performed for the compliance evaluation. One can notice the general trend for the three microstructures. The RM with pre-crack oriented into the transverse direction (RM T-S) is reaching higher forces and the decrease of the force during crack propagation is more progressive than for the two other configurations. FSPed material and rolled samples (RM L-S) start propagating the crack for a similar force level. However, the FSPed material fails suddenly, as the force drops down to 20% of the maximum force in a single crack propagation event.

Figure 8c describes the crack growth in the three displayed samples of Figure 8b. In good agreement with the observed trends, the RM T-S sample has a slower crack propagation rate compared to the other samples. Oppositely, in the FSPed sample the crack propagates 10 mm at once.

Figure 8d presents the K_{Ic} measurements obtained from the loading curves following the ASTM E399 standard. Mean values and standard errors are indicated. As plasticity is limited before crack propagation, the standard allows the computation of K_{Ic} (criterion $P_{max}/P_Q < 1.1$, with P_{max} the maximum force that can sustain the sample and P_Q the force at the onset of plasticity, according to ASTM E399). RM L-S samples pre-cracked in the rolling direction and FSPed specimens have the same fracture toughness K_{Ic} of 53 MPa√m, while the RM T-S samples pre-cracked in the transverse direction are showing a larger K_{Ic} value of 59 MPa√m.

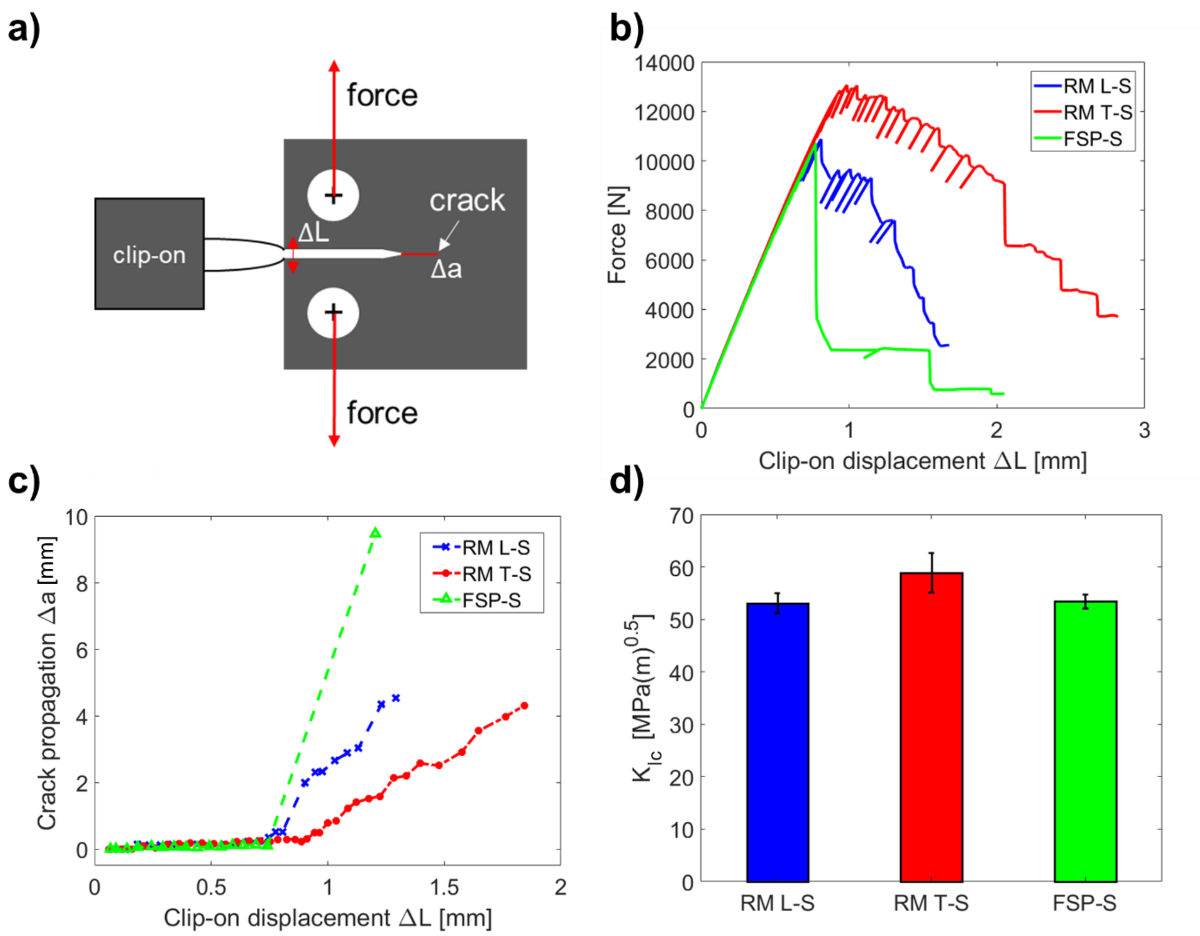

*Figure 8: CT samples results: **a)** sample geometry and parameters, **b)** loading curves of CT specimens, **c)** crack propagation with clip-on opening, **d)** toughness measurements. All samples are in T6 state.*

Figure 9 displays the broken surfaces of CT samples. Rolled material, i.e. RM T-S or RM L-S samples have a rough surface. Both rolled samples reveal secondary cracks propagating in the L-T plane. These secondary cracks propagate in an intergranular manner, following the elongated grains below the fracture surface. At higher magnification, dimples are visible on the cracked surfaces of Figure 9a-b, nucleated on intermetallic particles. Beside these ductile dimples, intergranular crack propagation is visible and associated to smooth darker regions, elongated along the L and T directions. Finally, a significant amount of the fracture surfaces is covered by small dimples, corresponding to a transgranular propagation of the main crack.

Figure 9c shows that FSPed material has a smoother surface, without macroscopic secondary crack nor obvious deviation. At higher magnifications, grain boundary decohesion as well as secondary intergranular cracks are evidenced on Figure 9c (bottom) for the FSPed microstructure (note the higher resolution for the FSPed alloy). A negligible amount of dimpled regions compared to RM samples is evidenced for the FSPed material (Figure 9c versus Figure 9a-b).

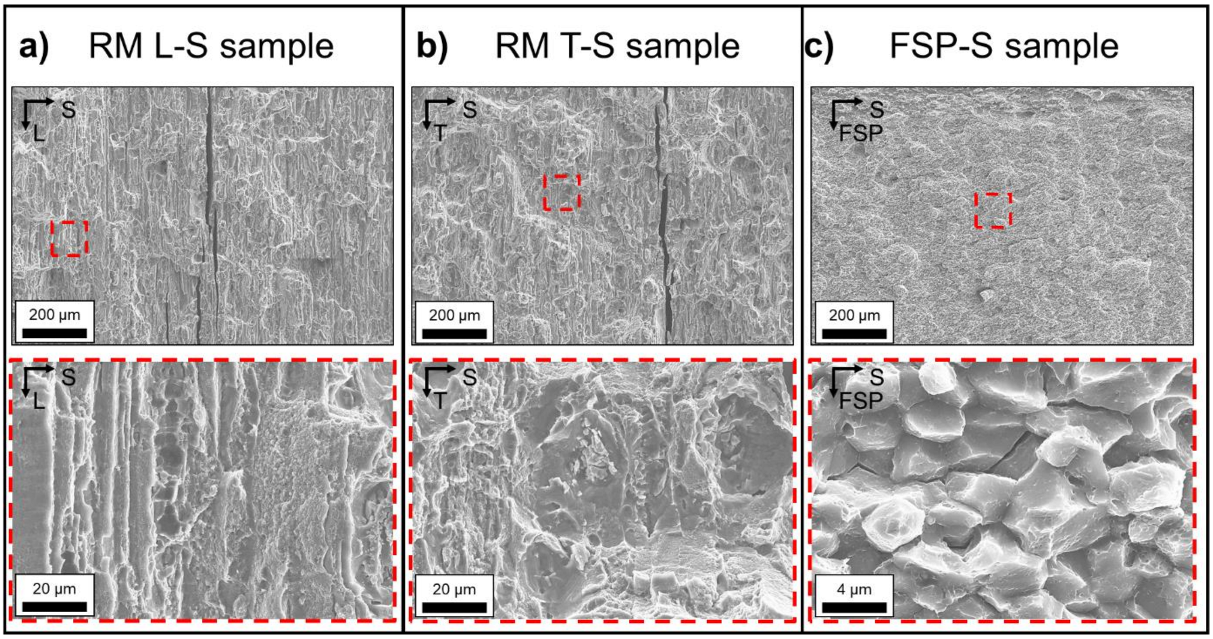

*Figure 9: Fracture surfaces of CT samples: **a)** crack propagation in L-S plane, low magnification identifies cracks propagating in the L-T plane, parallel to the loading direction, **b)** crack propagation in T-S plane, low magnification identifies cracks propagating in the T-L plane, parallel to the loading direction, **c)** crack propagation in FSPed-S plane, where some cracks are visible at high magnification, resulting from intergranular crack propagation. Red dashed boxes regions on top pictures are displayed at higher magnification on bottom. Note that the magnification of the bottom image of the FSPed material (c) is higher. The crack propagates from the top to the bottom of the figures. All samples are in T6 state.*

On Figure 10, CT samples are polished down to mid-thickness in order to highlight the crack propagation path. Figure 10a-b show the rolled material specimens, where elongated grains act as crack deviators or preferential propagation path depending on their orientation. Indeed, Figure 10a shows that for RM L-S sample, elongated grains are parallel to the crack propagation and lead to a flat crack along the grain boundary. Oppositely, in the RM T-S sample regular crack deviation and arrested cracks are visible. In that direction, each grain acts as a crack arrester, the main crack is thus regularly deviated. Figure 10c shows the FSP section at a 10 times higher magnification as the grains are much smaller than in the rolled samples. The crack path is thus following the grains, with a fully intergranular propagation but at a much smaller scale, limiting large-scale crack deviation.

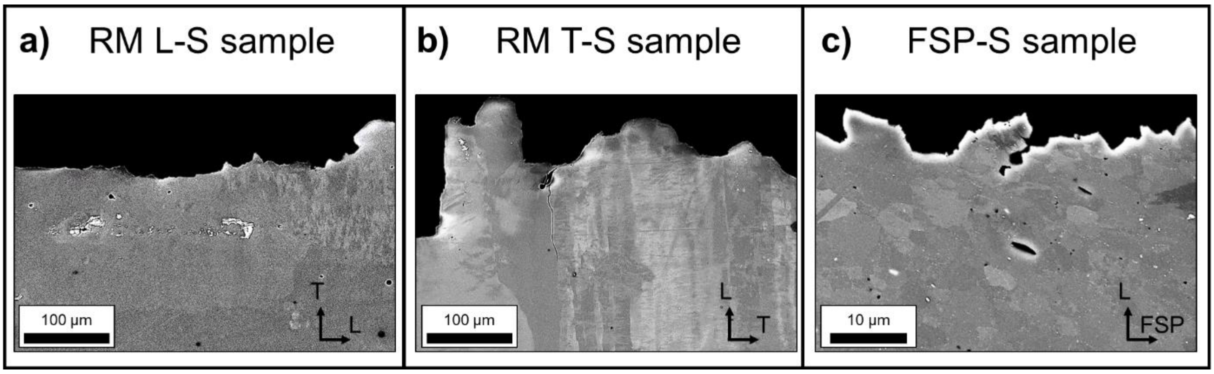

Figure 10: 2D cuts of broken CT specimens: ***a)*** *crack propagation in L-S plane, grain length is parallel to the crack propagation,* ***b)*** *crack propagation in T-S plane, grain length is perpendicular to the crack propagation,* ***c)*** *FSPed material, crack is parallel to the FSPed direction. Grains are significantly smaller and equiaxed on FSPed material, with a diameter of typically 3 µm. Note the higher magnification for FSPed material. The crack propagates from the right to the left of the figures. All samples are in T6 state.*

The broken surfaces of CT samples (as shown on Figure 9) are quantitatively analysed in Figure 11. Crack surfaces are processed in order to reveal the preferential orientations of the fracture surface (see Supplementary Figure S2 for methodology). As displayed on Figure 9, the fracture surface is influenced by the microstructure, i.e. the grain boundaries affect the fracture topology. The intergranular decohesion leads to smooth surfaces that can be detected as preferentially oriented features. On the opposite, transgranular propagation leads to rounded dimpled areas that are not preferentially oriented features. The intensity of the grain boundary intergranular crack propagation is thus quantified. For rolled materials, a 90° peak is visible in both L-S and T-S directions, corresponding to the crack propagation direction, parallel to the grains length and width respectively. The peak of the histogram is stronger in the RM L-S sample meaning that intergranular decohesion is more effective and / or more widespread than what is observed on RM T-S samples. Oppositely, the FSPed samples that show fully intergranular crack propagation presents a flat histogram. The absence of marked peak means that no specific intergranular propagation direction is identified on fracture surface, as the grains generate a randomly faceted surface.

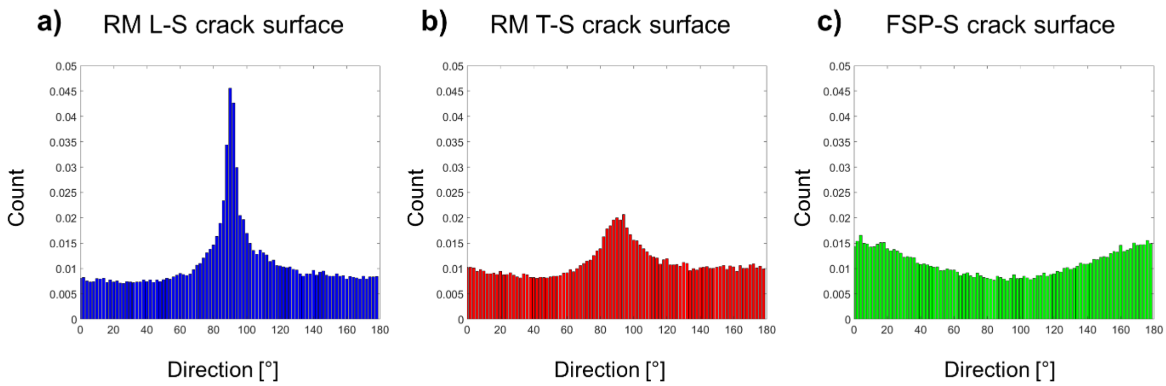

Figure 11: Directionality analysis of the three studied microstructures based on fracture surfaces of Figure 9. ***a)*** *RM L-S surface returns a strong peak centred at 90°, which is the rolling orientation,* ***b)*** *RM T-S surface generates a smaller peak at 90°, preferential orientation being less pronounced. Peak direction corresponds to the transverse direction,* ***c)*** *FSPed material lead to a flatter histogram, meaning that no specific preferential orientation is detected during the analysis. However, higher counts are centred at 0° orientation, i.e. the short direction.*

4. Discussion

4.1. Crack propagation in bending and CT samples: damage sequence and propagation mechanisms

CT pre-cracked samples allowed to calculate toughness (see Figure 8), which is relatively high for a 7XXX alloy (see Table 1), around 60 MPa√m for crack propagation along the transverse direction (RM T-S samples in Figure 8d). In parallel, bending samples highlight the formation of cracks from smooth surface and reveals the sharp crack tip structure inside the material in Figure 6 and Figure 7 respectively.

In what follows, crack propagation will be discussed, focussing first on the plastic deformation that prevails crack formation in the bending specimens.

First, crack propagation is dependent on the loading configuration as well as on the existence of a sharp crack tip [8][11]. Bending coupons are extensively plastically deformed before crack initiation, see Figure 12b and Figure 13b. Indeed, Figure 6 shows a significant amount of broken IM particles surrounding the cracked surface. This implies that a wide plastic zone is formed on hundreds of micrometres at the vicinity of the tensile surface, i.e. on the right part of the specimens in Figure 5, which is in accordance with [11]. No crack propagation is possible as long as no sharp crack has formed by ductile damage coalescence, retarding the sample failure. The main crack originates thus from the nucleated ductile damage (i.e. broken IM particles, see Figure 6), forming a 45° angle from the plate surface for all studied microstructures. This typical 45° orientation is related to a shear band as described by Ludtka *et al.* [6] and schematized on Figure 12b and Figure 13b.

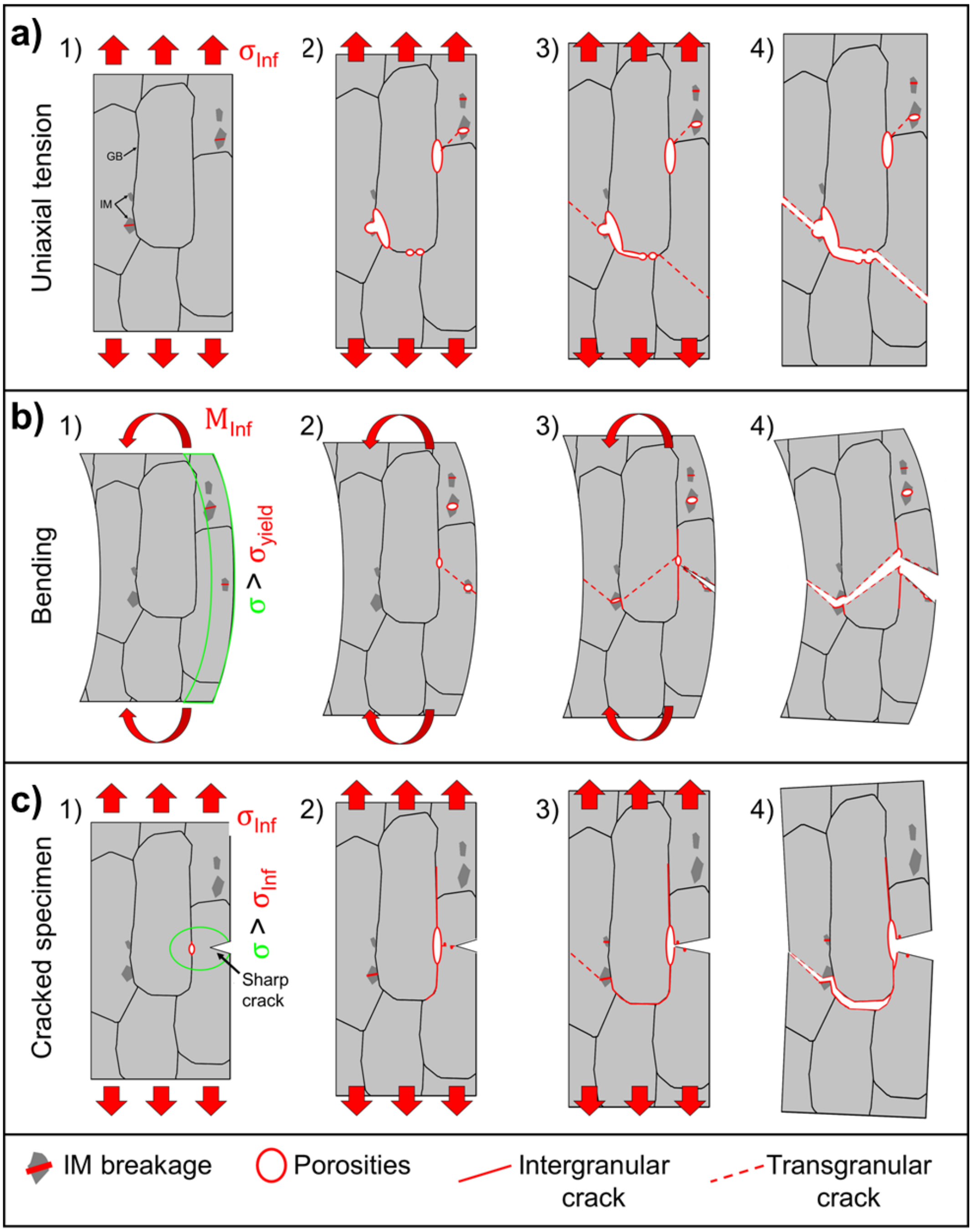

Figure 12: Damage mechanisms sequence in rolled alloy microstructure. ***a) Uniaxial tensile condition****. Damage nucleates on IM particles (1), intergranular decohesion occurs at grain boundary (2), transgranular damage propagation cuts the remaining ligaments (3), the broken sample shows mixed intergranular - transgranular crack path, containing some ductile dimples nucleated on broken IM particles.* ***b) Bending condition****. A plastic zone forms on the right of the bended material, leading to IM particles failure (1). The increasing bending localizes the deformation in a 45° shear band from the material surface towards nucleated porosities (2). Once the crack has formed, the propagation is partially deviated by the grain boundaries, before propagating in a transgranular fashion through the remaining grain ligaments (3). Finally, the crack shows a zigzag pattern, result of periodic intergranular crack deviation (4).* ***c) The rolled microstructure is pre-cracked****. Under loading, the stress rises near the crack tip, favouring ductile intergranular damage (1), damage propagates along the grain boundaries (2), the remaining grains arrests the cracks and fails by transgranular crack propagation, i.e. retarding crack advance (3), the final crack path is thus influenced by intergranular - transgranular propagation, containing broken IM particles.*

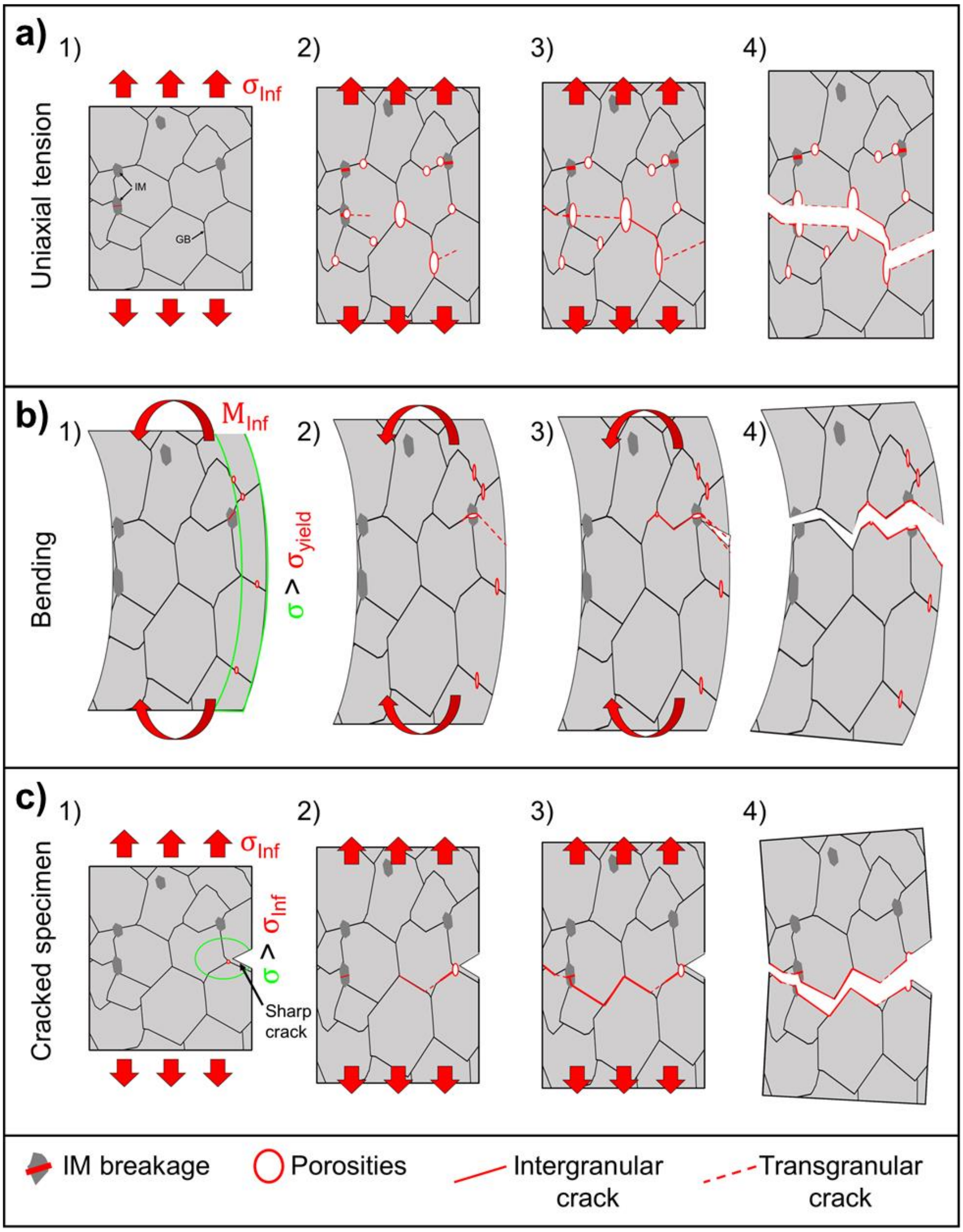

Figure 13: Damage mechanisms sequence in FSPed alloy microstructure. ***a) Uniaxial tensile condition****. Damage nucleates on remaining IM particles as well as at grain boundaries (2), porosities coarsen and are linked either by intergranular decohesion either by transgranular failure (3), the broken sample shows a mixed intergranular - transgranular crack path, containing some broken IM particles.* ***b) Bending condition.*** *A plastic zone forms on the right of the bended material, leading to IM particles failure and intergranular void nucleation (1). The increasing bending localizes the deformation in a 45° shear band from the material surface towards nucleated porosities (2). Once the crack has formed, it propagates following grain boundaries (3). Finally, the crack shows an intergranular dominated path (4).* ***c) The FSPed microstructure is pre-cracked****. Under loading, the stress rises near the crack tip, favouring intergranular damage (1), damage propagates along the grain boundaries (2), as grain boundary crack deviation is limited, extensive intergranular propagation leads to rapid crack propagation (3), the final crack path is thus mainly intergranular.*

Oppositely, propagation in CT samples occurs without extensive yielding, due to the sharp fatigue pre-crack, see Figure 12c and Figure 13c for rolled and FSPed microstructures respectively. This is in accordance with the literature [11]. As a proof of the limited yielding in CT samples, Figure 10 does not reveal any damage below the crack surface on the rolled alloys.

Once a first sharp crack is formed in the bended material, the propagation of the crack is similar to CT samples propagation. Indeed Figure 7 and Figure 10 show similar crack tortuosity and features in both bending and CT specimens.

On rolled alloy samples, a competition between two crack propagation mechanisms is observed, as displayed in Figure 12c. The first mechanism is grain boundary intergranular decohesion, as also identified by several authors [6][12][19]. Indeed, either on bending coupons or CT samples, cracks are sensitive to grain boundary orientation. Boundaries can deviate or facilitate the main crack propagation under loading depending on their orientation. The second mechanism is transgranular cutting of the grains. Grains that are not detached by grain boundary decohesion are cut transgranularly during crack propagation. The transgranular event generally leads to 45° tilted crack path that can be associated to failure of the grains by shearing [6]. It is obvious from Figure 9a-b that the crack surface is composed of these inter and transgranular damage propagation.

These two propagation mechanisms, either inter or transgranular, are acting together in the rolled materials, as described by Ludtka and Laughlin [6]. Figure 7a shows that the crack is discontinuous near the crack tip. In that region, coarse intergranular decohesion is visible at grain boundary while some elongated grains remain intact along the crack path. This indicates that the crack propagation is first driven by grain boundary decohesion in front of the crack and then by transgranular shearing of the remaining grains linking nucleated intergranular cracks, as schematized on Figure 12c.

Figure 9 reveals that extended intergranular cracks had propagated in the loading direction of the CT samples, i.e. in a direction perpendicular to the crack propagation (as schematized on Figure 12c). This is a proof that intergranular decohesion is a faster and easier damage path in the rolled microstructures, leading to delamination of the pancake shaped grains. Cracks will tend to follow the easiest path, even if the propagation direction is aligned with the loading direction. This is similar to observations made on laminated aluminium composites, where delamination occurs easily in the loading direction [23]. In accordance with laminate composites results of Cepeda-Jiménez *et al.* [23], the intergranular crack propagation of 7475 rolled material acts like the delamination of rolled bond composites. In both cases, toughness is increased due to crack deviation.

4.2.Rolled material anisotropy

Limiting the intergranular easy propagation is thus associated to higher crack resistance and toughness in 7XXX materials. The rolled microstructure composed of elongated grains has anisotropic behaviour, in terms of tensile and toughness properties (see Table 3 and Figure 8d respectively). The RM T-S samples have higher toughness compared to the RM L-S specimens of Figure 8d, as observed and described by Iriç *et al.* [15] on 7075 alloy. Crack propagation along the transverse direction is harder than along the rolling direction. A similar behaviour is observed in bending: the cracks propagate more easily for tensile stresses along the transverse direction, i.e. RM L-S sample has lower bending angle (Figure 4). This is in good agreement with the lower crack propagation resistance of the RM L-S sample (i.e. loading along the transverse direction). Note that despite similar crack propagation planes (L-S, T-S and FSP-S), the CT and bending samples propagate the cracks in different directions. Indeed, cracks in all bending specimens propagate from the tensile surface in the short (S) direction, while cracks in CT specimens propagate along the rolling (RM L-S), transverse (RM T-S) and FSPed (FSP-S) directions respectively (see Figure 1). The crack plane containing the rolling (L) direction is thus the weakest independently of the crack propagation direction.

Despite higher K_{Ic} for RM T-S material, the fractography images of Figure 9a-b display both intergranular and transgranular crack propagation for RM T-S and RM L-S specimens. The influence of grain orientation is more obvious on Figure 10. Tortuosity of the crack is higher for the RM T-S compared to RM L-S. The higher K_{Ic} value is thus associated to that higher tortuosity, even if similar intergranular versus transgranular mixed crack propagation was observed for both orientations. Interestingly, both RM L-S and RM T-S bending samples show tortuous cracks on Figure 5. The RM L-S specimen shows large intergranular decohesion at crack tip vicinity, associated to mixed mode crack propagation (Figure 7a). Oppositely, the orientation of grains in the RM T-S sample favours transgranular propagation, as the grains main axis is perpendicular to the crack propagation direction. Only limited intergranular decohesion is evidenced on the RM T-S bending sample, as visible on Figure 7b. The grain orientation in front of the crack is thus influencing both tortuosity of the crack path and the intergranular versus transgranular propagation mechanism.

The influence of intergranular crack propagation can be estimated on the fracture surface using the analysis of Figure 11. The preferentially oriented features are parallel to the crack propagation direction i.e. oriented at 90°. Peaks observed in Figure 11a-b are not equivalent, meaning that the RM L-S specimens show more widespread and/or numerous patterns on the crack surface. The highest peak in the histogram is associated to more aligned intergranular propagation. The cracks can thus propagate more easily into the material as no crack arrester deviates the intergranular decohesion in the rolling direction. Oppositely, the RM T-S specimens are still affected by 90° oriented intergranular crack propagation but these zones are shorter and/or less numerous, as the grain shape is able to induce deviation that retards the cracking and forces the crack to cross the tougher grain interior.

4.3. Influence of the FSP + T6 HT on crack propagation

The FSP material is showing exceptional ductility upon uniaxial loading, as recalled in Table 3. However, the FSPed and rolled materials present similar bending properties. More surprisingly, K_{Ic} for FSPed material is lower than for RM T-S rolled material (see Figure 8d). Low crack propagation resistance of FSPed material (see Figure 8b) contrasts with the higher ductility measured in our previous work [19]. The damage sequence in uniaxial loading of FSPed T6 material is described in Figure 13a. The following paragraphs will discuss the possible reasons of such unexpected low performances of the FSPed T6 microstructure.

The first reason is related to the modification of the crack propagation mechanism despite similar PFZ width and hardening precipitates in both rolled and FSPed materials [19]. The FSPed microstructure is associated to extensive intergranular propagation, as displayed on Figure 13c. A toughness decrease in 7XXX alloys was already associated to a change in fracture mechanism [6]. The higher the amount of intergranular crack propagation, the less tough is the material [6], see Table 1. The intergranular dominated propagation reduces the crack propagation resistance but to the best of the authors' knowledge, it was never described on refined FSPed microstructure.

However, our previous study [19] proved that grain size and shape are affecting damage mechanisms in uniaxial loading, by limiting or facilitating intergranular decohesion, see Figure 12a and Figure 13a. In particular, the FSPed material in T6 state showed a retarded damage, increasing the strain needed for damage coalescence (Figure 13a). Surprisingly, the refined FSPed microstructure is leading to mixed mode intergranular and transgranular damage propagation, at extremely high strains compared to rolled material.

The higher ductility of FSPed T6 microstructure is mainly related to the reduction of IM particles size and the redistribution of IM clusters inside the alloy matrix. Such modification to the IMs increases the strain required for IM particle fracture or decohesion, as shown in our previous work [19]. The higher ductility after FSP was also observed on 6XXX series by Hannard *et al.* [24], and also associated to a refinement of the brittle IM particles and homogenization of the IM clusters in the matrix. A quantification of the IM particles and IM clusters and their influence on fracture mechanisms was also performed by Hannard *et al.* [20]. Their results are in good agreement with the results obtained in the present work.

Secondly, it was shown that elongated grains of the rolled alloy are more prone to early damage initiation due to the straight grain boundaries (Figure 12a), while FSPed refined grains were not showing any early intergranular damage initiation before reaching higher strains (Figure 13a).

However, in a crack propagation sample like CT specimens (or bending specimens after crack initiation), the existence of a sharp crack tip changes the conditions, i.e. increasing significantly the triaxiality. The resistance to crack propagation will be higher with more deviation and crack arresters. The elongated rolled grains are efficient for retarding crack propagation, if the crack direction is perpendicular to the grains (Figure 12c). Oppositely, cracks follow easily the FSPed grains, and the intergranular propagation covers most of the propagation surface on Figure 9c (see schematic on Figure 13c). Oppositely, the rolled material retains a mixed inter versus transgranular mode of propagation. Indeed, cut grains are clearly visible in Figure 9a-b. This is nicely correlated to Wang *et al.* [16] results that demonstrated the intergranular crack propagation tendency of recrystallized grains on rolled material.

A second consideration is the following. Despite easy crack propagation, the bending curve of the FSPed material is similar to the best configuration for the rolled material loading, i.e. RM T-S sample. We can now make sense of this apparent incoherency with the CT loading results in which the rolled materials have significantly higher crack propagation resistance (Figure 8c). Indeed, during the bending of FSPed material, the crack initiation is delayed compared to the rolled microstructure as the stress configuration is similar to uniaxial loading on the bended free surface (Figure 13b), in accordance with Lezaack *et al.* [19] ductility improvement under uniaxial loading (Figure 13a). Oppositely, propagation is very fast after crack opening, leading to rapid failure of the sample (Figure 13c) as the propagation is fully intergranular. These two effects play opposite roles on failure, which explains the relatively high reached bending angle in FSPed material despite fast intergranular propagation.

4.4. A pathway towards high performance 7XXX alloys

According to the presented results and the ductility improvement reported in Lezaack *et al.* [19], the ideal microstructure for both tough and ductile 7XXX alloys at full T6 strength can be discussed. FSPed microstructure has a higher ductility because of the crack initiation delay, as damage is nucleating at higher strains. The smaller size of IM particles is the most important damage tempering effect. However, the FSP microstructure does not resist crack propagation efficiently in comparison with the rolled material when the orientation is favourable, as proved by K_{Ic} measurements of Figure 8d. Small grains favour a near 100% intergranular propagation, leading to low energy absorption during crack propagation.

The ideal microstructure should thus have a reduced IM particles content and smaller IM particles sizes in order to temper damage initiation or crack nucleation. In parallel, grain structure and size should be tuned for crack propagation resistance. Coarse and elongated grains of the rolled material are able to resist crack propagation by crack deviation and transgranular ductile propagation. However, rolled material behaviour is not isotropic, delamination occurs easily along the plate thickness (T-L plane propagation). Indeed, grain boundaries of the elongated grains are preferential damage sites, leading to lower toughness when boundaries are aligned with the crack propagation direction. This is why the toughness of the rolled material RM L-S is lower than for the opposite crack direction in RM T-S samples, see Figure 8d.

The ideal microstructure should be composed of grains that should be sufficiently large for imposing large crack deviation and thus favouring transgranular propagation. In order to reduce the anisotropy, the grain boundaries should be more randomly oriented to prevent the formation of a preferential damage propagation direction. Randomly oriented grains interlocked in each other should be efficient for arresting cracks in all directions, avoiding preferential crack propagation as observed on rolled microstructure of Figure 9a-b. Figure 14 proposes a schematic of such an ideal microstructure. Elongated grains assembled in packets, have random orientation and can deviate the crack at each new packet orientation. The challenge is now to manufacture such a microstructure.

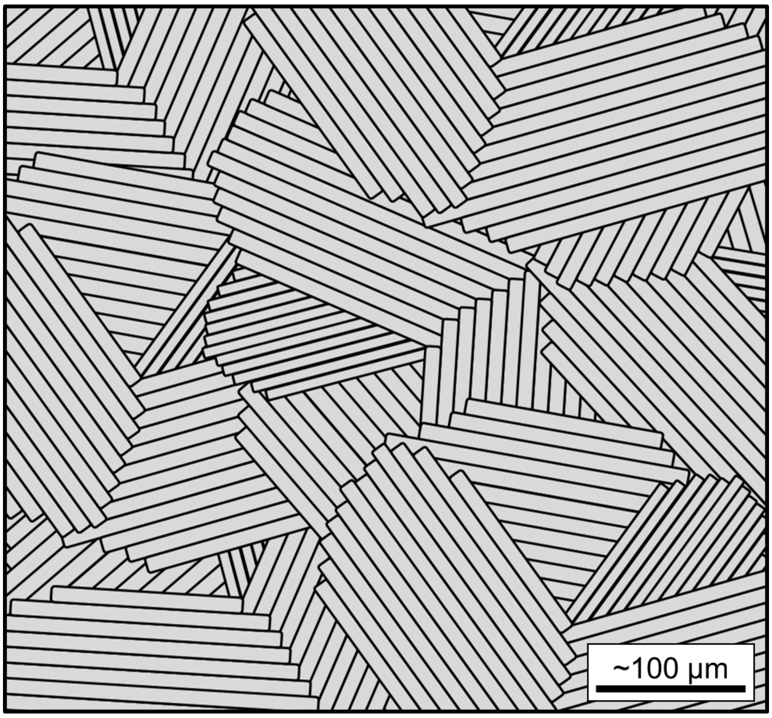

Figure 14: Illustration of a new microstructure for improving toughness and ductility in 7XXX alloys: elongated and randomly distributed grains increase the crack propagations resistance in a more isotropic fashion, by enforcing intergranular deviation at each new grain orientation, which is not possible on current rolled 7XXX alloys because of the preferential orientation of the grains in the rolling direction.

5. Conclusions

FSPed and rolled materials have been tested under bending and compact tension loading, providing failure bending angles and K_{Ic} values. While FSP significantly increases the ductility under uniaxial tension, FSP is found to reduce the rolled material toughness. Indeed, the small FSP grains favour fast intergranular crack propagation. Rolled microstructure retards efficiently crack propagation due to crack deviation and enforced transgranular damage. Depending on rolled material orientation, the alignment of grain boundaries with the crack propagation direction is reducing the bending angle and the toughness. Toughness anisotropy of rolled microstructure is a limitation in applications.

The FSP grain structure is more equiaxed, limiting material anisotropy. Despite lower crack resistance by crack deviation, its K_{Ic} value is still close to the rolled material in the less favourable crack propagation direction. FSP refines IM particles leading to a bending angle equivalent to the favourable direction in the rolled microstructure. Crack initiation is retarded on the FSP microstructure, as evidenced by uniaxial loading.

Based on these considerations, authors propose that toughness and ductility can be concomitantly enhanced in 7XXX alloys by playing on the right parameters: iron-rich intermetallic particles (size and content) as well as grain shape and size. Intermetallic particles characteristic size and clustering should be reduced as much as possible for damage and crack nucleation delay, as demonstrated on FSPed microstructure, while grains should be as elongated as classical rolled grains and randomly oriented for generating crack deviation.

Acknowledgements

This research work has been supported by the European Research Council (ERC) under the European Union's Horizon 2020 research and innovation program (grant agreement n716678). M.B.L. and F.H. are mandated by the Belgian National Fund for Scientific Research (FSR-FNRS).

Data availability

The raw/processed data required to reproduce these findings cannot be shared at this time as the data also forms part of an ongoing study.

ASTM E1820-2011. Standard test method for measurement of fracture toughness.

References

[1]. J.-Q. Su, T.W. Nelson, R. Mishra, M. Mahoney, Microstructural investigation of friction stir welded 7050-T651 aluminium, Acta Materialia 51, (2003) 713-729.

[2]. Y. Wang, X. Wu, L. Cao, X. Tong, Y. Zou, Q. Zhu, S. Tang, H. Song, M. Guo, Effect of Ag on aging precipitation behavior and mechanical properties of aluminum alloy 7075, Materials Science and Engineering A 804, (2021) 140515.

[3]. S. Liu, Q. Li, H. Lin, L. Sun, T. Long, L. Ye, Y. Deng, Effect of quench-induced precipitation on microstructure and mechanical properties of 7085 aluminum alloy, Materials and Design 132, (2017) 119-128.

[4]. P.A. Rometsch, Y. Zhang, S. Knight, Heat treatment of 7xxx series aluminium alloys - Some recent developments, Transactions of Nonferrous Metals Society of China 24, (2014) 2003-2017.

[5]. B. Milkereit, M.J. Starink, P.A. Rometsch, C. Schick, O. Kessler, Review of the quench sensitivity of aluminium alloys: Analysis of the kinetics and nature of quench-induced precipitation, Materials 12, (2019) 4083.

[6]. G. M. Ludtka, D. E. Laughlin, The influence of microstructure and strength on the fracture mode and toughness of 7XXX series aluminum alloys, Metallurgical Transactions A 13, (1982) 411-425.

[7]. B. Zhou, B. Liu, S. Zhang, The advancement of 7XXX series aluminum alloys for aircraft structures: A review, Metals 11, (2021) 718.

[8]. H.A. Wood, R.M. Engle Jr, USAF Damage Tolerant Design Handbook: Guidelines for the analysis and design of damage tolerant aircraft structures, Technical Report AFFDL-TR - Air Force Flight Dynamics Laboratory 3021, (1979).

[9]. Y. Zhu, K. Sun, G.S. Frankel, Intermetallic phases in aluminum alloys and their roles in localized corrosion, Journal of The Electrochemical Society 165, (2018) 807-820.

[10]. X.-M. Li, M.J. Starink, Effect of compositional variations on characteristics of coarse intermetallic particles in overaged 7000 aluminium alloys, Materials Science and Technology 17, (2001) 1324-1328.

[11]. M. Vratnica, G. Pluvinage, P. Jodin, Z. Cvijović, M. Rakin, Z. Burzić, K. Gerić, Notch fracture toughness of high-strength Al alloys, Materials and Design 44, (2013) 303-310.

[12]. N. Kamp, I. Sinclair, M.J. Starink, Toughness-strength relations in the overaged 7449 Al-based alloy, Metallurgical and Materials Transactions A 33, (2002) 1125-1136.

[13]. F. Scheyvaerts, P.R. Onck, Y. Bréchet, T. Pardoen, Multiscale simulation of the competition between transgranular and intergranular ductile fracture, 11th International Conference on Fracture 6, (2005) 4164-4169.

[14]. M. Tajally, Z. Huda, H.H. Masjuki, A comparative analysis of tensile and impact-toughness behavior of cold-worked and annealed 7075 aluminum alloy, International Journal of Impact Engineering 37, (2010) 425-432.

[15]. S. Iriç, A.O. Ayhan, Dependence of fracture toughness on rolling direction in aluminium 7075 alloys, Acta Physica Polonica A 132, (2017) 892-895.

[16]. Y. Wang, X. Wu, L. Cao, X. Tong, M. J. Couper, Q. Liu, Effect of trace Er on the microstructure and properties of Al-Zn-Mg-Cu-Zr alloys during heat treatments, Materials Science and Engineering A 792, (2020) 139807.

[17]. R.S. Mishra, Z.Y. Ma, Friction stir welding and processing, Materials Science and Engineering R 50, (2005) 1-78.

[18]. F. Zhang, X. Su, Z. Chen, Z. Nie, Effect of welding parameters on microstructure and mechanical properties of friction stir welded joints of a super high strength Al-Zn-Mg-Cu aluminum alloy, Materials and Design 67, (2015) 483-491.

[19]. M. B. Lezaack, F. Hannard, L. Zhao, A. Orekhov, J. Adrien, A. Miettinen, H. Idrissi, A. Simar, Towards ductilization of high strength 7XXX aluminium alloys via microstructural modifications obtained by friction stir processing and heat treatments, Materialia 20, (2021) 101248.

[20]. F. Hannard, A. Simar, E. Maire, T. Pardoen, Quantitative assessment of the impact of second phase particle arrangement on damage and fracture anisotropy, Acta Materialia 148, (2018) 456-466.

[21]. M. B. Lezaack, A. Simar, Avoiding abnormal grain growth in thick 7XXX aluminium alloy friction stir welds during T6 post heat treatments, Materials Science and Engineering A 807, (2021) 140901.

[22]. J. Schindelin, I. Arganda-Carreras, E. Frise, V. Kaynig, M. Longair, T. Pietzsch, S. Preibisch, C. Rueden, S. Saalfeld, B. Schmid, J.-Y. Tinevez, D.J. White, V. Hartenstein, K. Eliceiri, P. Tomancak, A. Cardona, Fiji: an open-source platform for biological-image analysis, Nature Methods 9, (2012) 676-682.

[23]. C.M. Cepeda-Jiménez, P. Hidalgo, M. Pozuelo, O.A. Ruano, F. Carreño, Influence of constituent materials on the impact toughness and fracture mechanisms of hot-roll-bonded aluminum multilayer laminates, Metallurgical and Materials Transactions A 41, (2010) 61-72.

[24]. F. Hannard, S. Castin, E. Maire, R. Mokso, T. Pardoen, A. Simar, Ductilization of aluminium alloy 6056 by friction stir processing, Acta Materialia 130, (2017) 121-136.

Supplementary data

CT samples geometry

CT test samples geometry is detailed on Figure S1.

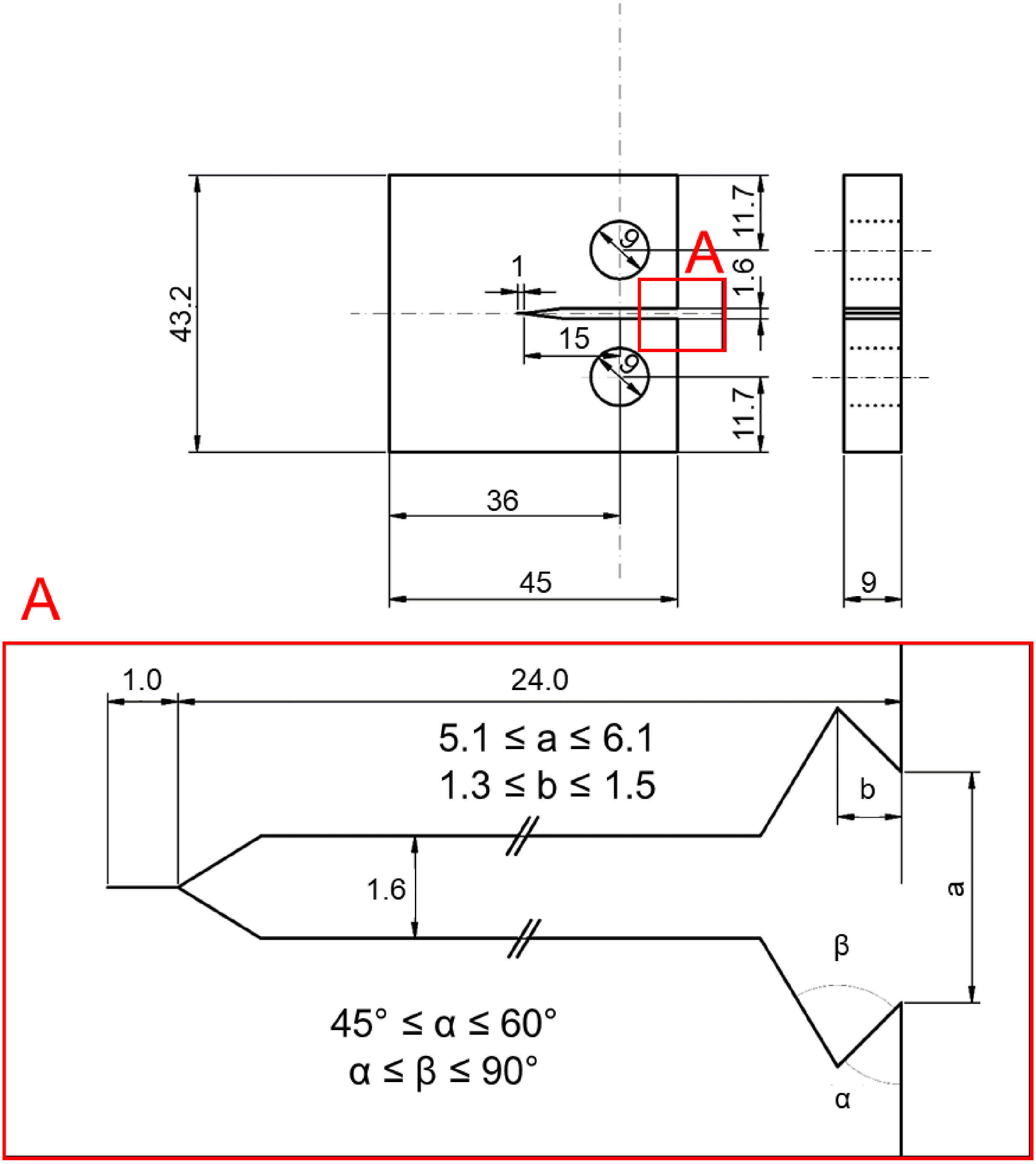

Figure S1: CT geometry. Units: mm.

Directionality analysis

The ImageJ 'Directionality' analysis method is described in this section. ImageJ software is available on https://imagej.net/ and the Directionality method is described in https://imagej.net/plugins/directionality#references. Images are chopped into square fragments. A Fourier spectrum analysis is performed on each square and then filtered to compute the intensity of the aligned features of the initial image. A histogram is generated, taking into account the amount of features parallel to the angles oriented between 0 and 180°.

Figure S2 illustrates the application of the analysis to simple squared patterns: striped texture in **a)** and **b)** are leading to a strong peak corresponding to the stripes orientation. When mixed texture is analysed, in **c)**, two-peaks are resulting from the analysis. If an image presents a dominant orientation, like in **d)**, this orientation will lead to the highest peak.

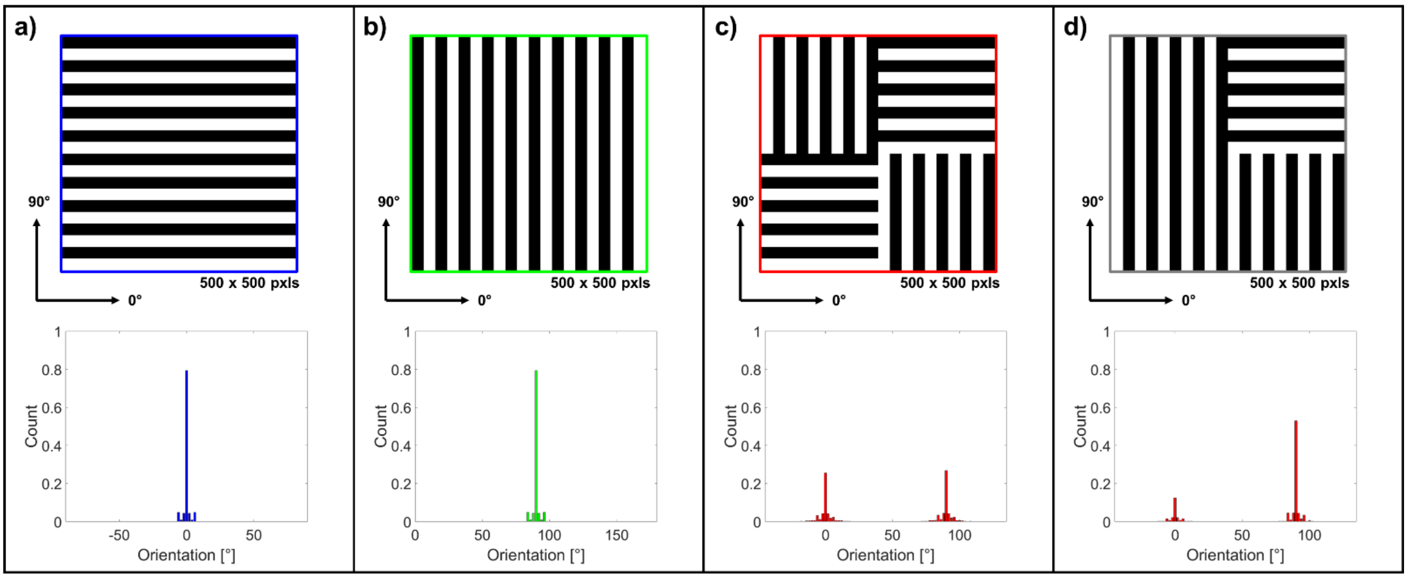

*Figure S2: Image analysis, using Directionality plugin of ImageJ software. **a)** A 500 × 500 pixels striped image is analysed by the plugin, leading to a strong peak at 0° orientation. **b)** Same as (a), with vertical stripes, leading to a 90° peak in the histogram. **c)** A mixed structure with equivalent proportions of horizontal and vertical stripes leads to a 2-peaked histogram, at 0° and 90° orientations. **d)** Mixed microstructure with 75 % vertical stripes, leading to larger peak in 90° orientation and a smaller peak around 0° orientation.*